J Electroceram (2008) 21:49–54
DOI 10.1007/s10832-007-9083-9

Ferroelectric distortion and electronic structure in $Bi_4Ti_3O_{12}$

Yuji Noguchi · Takashi Goto · Masaru Miyayama · Akinori Hoshikawa · Takashi Kamiyama

Published online: 21 March 2007

Abstract The ferroelectric phase transition in $Bi_4Ti_3O_{12}$ has been investigated through Rietveld analysis of high-resolution neutron powder diffraction and electronic structure calculations. The structural and electronic analyses show that the traditional model based on the stereoactive lone-pair 6*s* electrons of Bi^{3+} is not sufficient to explain the structural distortions in the ferroelectric state. It is strongly suggested that the hybridization of the Bi 6*p* and the O 2*p* in the perovskite layers is the trigger of the ferroelectric transition in $Bi_4Ti_3O_{12}$, and that this orbital interaction is responsible for stabilizing the ferroelectric displacements in the perovskite layers.

Keywords Ferroelectric phase transition · Rietveld analysis · Perovskite layers

1 Introduction

The study of ferroelectrics offers opportunities to advance the fundamental physics and materials design of dielectric materials, and to develop innovative semiconductor-based applications such as nonvolatile memories, piezoelectric and electro-optic devices and uncooled infrared detectors. [1] Ferroelectric bismuth titanate ($Bi_4Ti_3O_{12}$, BiT) [2] has been regarded as a promising material because of its high Curie temperature (T_C) of 675 °C [3], and large spontaneous polarization (P_s) of ~50 μC/cm^2 [4, 5] as well as large electro-optic coefficients [6, 7].

In the crystal structure of BiT, the perovskite layers composed of three TiO_6 octahedral layers with Bi at the *A* site are sandwiched between Bi_2O_2 layers, as shown in Fig. 1. In the paraelectric state above T_C, BiT has a parent tetragonal structure with *I*4/*mmm* symmetry. The ferroelectric transition results in descending symmetry to monoclinic *B*1*a*1 space group. [8] Polarization measurements of BiT single crystals have revealed a P_s of 50 μC/cm^2 along the *a* axis and of 3–5 μC/cm^2 along the *c* axis. [4, 5] Rae et al. [8] have clearly shown through single-crystal structural analysis at room temperature that the shape of TiO_6 octahedra in the paraelectric state remains nearly intact in the ferroelectric state. The TiO_6 octahedra rotate in the *a*–*b* plane as well as incline away from the *c* axis. The ferroelectricity of BiT originates from the relative *a*-axis displacement of Bi at the *A* site with respect to the TiO_6 octahedra, and the off-center Ti displacements in the octahedra play a minor role in P_s. [8] These structural features of BiT are completely different from the ABO_3-type ferroelectrics such as $BaTiO_3$ and $PbTiO_3$ where the ferroelectricity is induced by the relative displacements of *A* and *B* cations with respect to oxygen-octahedral cage. Recently, rare-earth substituted BiT [9, 10] has attracted a great deal of attention, because it shows a superior remanent polarization with high fatigue endurance in the form of thin films with metal electrodes. [11–14, 15]

For several decades, the crystal structure of BiT has been investigated to elucidate the origin of ferroelectricity. [8, 9,

The author Akinori Hoshikawa is already deceased

Y. Noguchi (✉) · T. Goto · M. Miyayama
RCAST, The University of Tokyo,
4-6-1, Komaba, Meguro-ku,
Tokyo 153-8904, Japan
e-mail: ynoguchi@crm.rcast.u-tokyo.ac.jp

Y. Noguchi
PRESTO, Japan Science and Technology Agency,
4-1-8, Honcho,
Kawaguchi, Saitama 332-0012, Japan

A. Hoshikawa · T. Kamiyama
Neutron Science Laboratory, Institute of Materials Structure Science, High Energy Accelerator Research Organization,
1-1 Oho, Tsukuba,
Ibaraki 305-0801, Japan

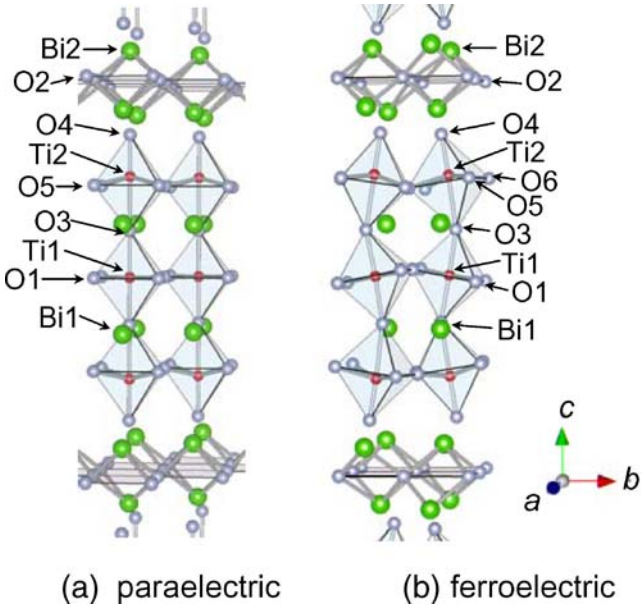

Fig. 1 Actual crystal structures of (**a**) the paraelectric phase at 700 °C and (**b**) the ferroelectric phase at 25 °C

16–22] Dorrian et al. [9] proposed a model that the correlated reorientation of lone-pair electrons associated with Bi^{3+} results in the monoclinic distortion. Several authors [16–19, 21, 22] have argued that the lone-pair electrons in the Bi^{3+} 6*s* orbitals play an essential role in the structural distortions in the ferroelectric state. Withers et al. [17] have analyzed the bond valence from the structural data and concluded that the ferroelectricity results from gross underbonding of Bi1 at the perovskite *A* site in the undistorted paraelectric structure. Hervoches et al. [20] have conducted a high-temperature powder neutron diffraction study, and demonstrated that the driving force of the ferroelectric phase transition is the requirement for Bi1 to optimize its bonding to the neighboring oxide ions.

In the present study, the ferroelectric phase transition of BiT has been investigated through structural analysis and electronic band structure calculations. It is shown that the traditional model [16–19, 21, 22] based on the stereoactive lone-pair 6*s* electrons of Bi^{3+} is not sufficient to explain the structural distortion in the ferroelectric state. These structural and electronic analyses demonstrate that the hybridization of the Bi 6*p* and O 2*p* in the perovskite layers acts as a trigger of the ferroelectric transition and stabilizes the ferroelectric distortions in the perovskite layers.

2 Experimental procedure

Powder samples of BiT were prepared by a solid-state reaction for diffraction measurements. [23, 24] The raw materials of Bi_2O_3 and TiO_2 of 99.99% purity were thoroughly mixed with the stoichiometric composition, and dried using a rotary evaporator. The mixture was calcined at 800 °C for 4–8 h in air with intermediate grindings. This procedure led to a single phase of BiT.

Time-of-flight neutron powder diffraction data were collected at 25 °C and at 700 °C using the *Sirius* diffractometer at KENS [25], and a vacuum furnace was used for high-temperature measurements. In the structure analyses, a backward bank that has the best resolution (0.25%) with high reliability was used. Structural parameters were refined by the Rietveld method using the program RIETAN-TN [26]. Although BiT has a *B*1*a*1 monoclinic symmetry in the ferroelectric state, the monoclinic distortion is very small, and the monoclinic angle has been reported to be 90°. [8] Indeed, in our analysis, the structure refinement based on *B*1*a*1 gave almost the same *R* factors as the case based on *B*2*cb* orthorhombic symmetry. Thus, we investigated the crystal structure of ferroelectric BiT in the *B*2*cb* orthorhombic system. For the data obtained at 700 °C, the analysis based on *I*4/*mmm* tetragonal symmetry led to smaller *R* factors compared with that on the orthorhombic one.

We calculated the electronic band structure and electronic density of states (DOS) of BiT for the low-temperature ferroelectric and the high-temperature paraelectric phases. The calculations were performed within density functional theory via the generalized gradient approximation [27, 28] using a plane wave basis set. The projector-augmented wave (PAW) method [29, 30] was applied using the Vienna Ab-initio Simulation Package (VASP) [31]. The cutoff energy of 400 eV and Monkhorst-Pack *k*-point sampling grid of 7×7×3 were used. The structure data determined by the Rietveld analysis were used for calculating the electronic band structures.

3 Results and discussion

3.1 Structure analysis

Figure 2 shows the results of the Rietveld analysis for (a) low-temperature ferroelectric (25 °C) and (b) high-temperature paraelectric (700 °C) phases. The final calculated profiles fit fairly well with the experimental data for both phases. In our analysis, *R*-weighted pattern (R_{wp}) was small (1–4%) and goodness of fit indicator (*S*) was closed to one (1.1–1.5). The refined lattice parameters at 25 °C were *a*= 0.544 587(6) nm, *b*=0.540 770(6) nm, and *c*=3.282 70 (5) nm, which are consistent with the results of single-crystal structural analysis performed by Rae et al. [8]

Here, we consider ionic displacements and the resultant spontaneous polarization (P_s). In the ferroelectric state, the TiO_6 octahedra rotate in the *a*–*b* plane as well as incline away from the *c* axis. [8, 15, 21] These octahedral

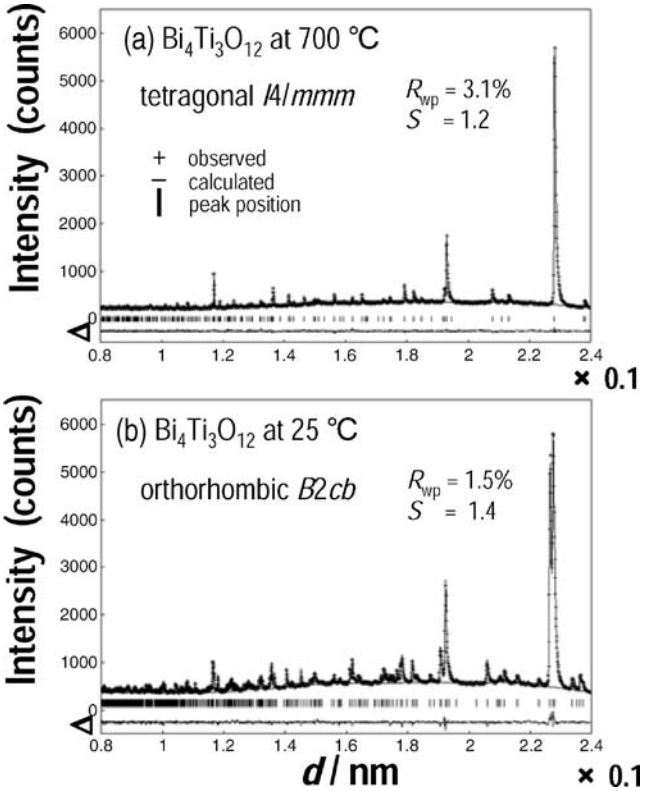

Fig. 2 Results of the Rietveld analysis of the powder neutron diffraction at (**a**) 700 °C and (**b**) 25 °C. *Delta symbol* indicates the difference between calculated and experimental intensities

distortions induce many kinds of displacive-type ferroelectric soft modes. The dipole moments caused by the ionic displacements along the *b* axis are cancelled due to the presence of glide plane normal to the *b* axis. Thus, the constituent ions are displaced cooperatively only along the *a* and *c* axes, leading to a spontaneous polarization (P_s) along both axes. It has been reported that the P_s along the *a* axis is ~50 μC/cm^2, [4, 5, 15] which is much larger than that along the *c* axis (3–5 μC/cm^2 [4]). Hereafter, we pay attention only to the P_s along the *a* axis.

Assuming the constituent ions to have their formal charge (+3 for Bi, +4 for Ti, −2 for O), we can calculate the ionic spontaneous polarization ($P_{s,\,ion}$) by the following equation:

$$P_{s,\,ion} = \sum_i (m_i \times \Delta x_i \times Q_i e)/\Omega, \quad (1)$$

where m_i is the site multiplicity, Δx_i is the displacement along the *a* axis from the corresponding position in the parent tetragonal (*I*4/*mmm*) structure, $Q_i e$ is the ionic charge for the *i*th constituent ion, and Ω is the volume of the unit cell. Figure 3 depicts (a) the actual crystal structure at 25 °C projected along the *b* axis, (b) the Δx_i along the *a* axis, and (c) the dipole moment $(m_i \times \Delta x_i \times Q_i e)/\Omega$. It is interesting to note that three TiO_6 octahedral layers move cooperatively along the *a* axis with respect to the Bi ions, which lead to a $P_{s,ion}$ opposite to the *a* axis. In our analysis, $P_{s,ion}$ was estimated to be 37.6 μC/cm^2 at 25 °C. This value is smaller than that of the experimental P_s, because electronic contribution is not taken into account in the calculation of $P_{s,ion}$. [32] Although relative displacements of the Ti ions with respect to the TiO_6 octahedral center were observed, the off-center Ti displacements play a minor role in $P_{s,\,ion}$. The entire shift of the TiO_6 octahedra with respect to the Bi ions results in the large dipole moments of the oxide ions in the perovskite layers, which gives the dominant contribution to the ferroelectric polarization in the BiT system [see Fig. 3(c)].

3.2 Electronic density of states

Figure 4 shows the electronic density of states (DOS) for the ferroelectric (25 °C) and paraelectric phases (700 °C) calculated from the structural data determined by the Rietveld analysis. In the DOS spectra, the Fermi level (E_F) is set at 0 eV. In the paraelectric state, the fundamental E_g is indicated to be indirect (valence band maximum at the *P* and conduction band minimum at the Brillouin-zone center Γ). This is consistent with the calculation performed by Shimakawa et al. [21] In contrast, our calculations suggest that the ferroelectric BiT has a direct band gap, where the valence band maximum and conduction band minimum lie at the Γ. For both the paraelectric and ferroelectric phases, the Bi 5*d* states are localized at a deep level (−22 to −24 eV). The O 2*s* and Bi 6*s* stats appear at −17 to −20 eV and −7 to −12 eV, respectively. The valence band consists mainly of the O2*p* states, while the Ti 3*d*

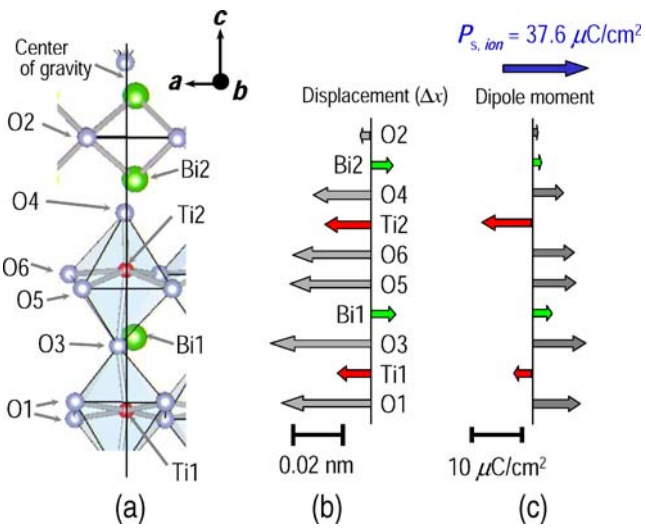

Fig. 3 Detailed structural distortion at 25 °C along the polarization direction (the *a* axis); the actual crystal structure projected along the *b* axis, (**b**) the atomic displacement (Δ*x*) along the *a* axis from the corresponding position in the parent tetragonal (*I*4/*mmm*) structure and (**c**) the dipole moment obtained from the Δ*x* and formal charge. The $P_{s,ion}$ along the *a* axis at 25 °C was estimated to be 37.6 μC/cm^2

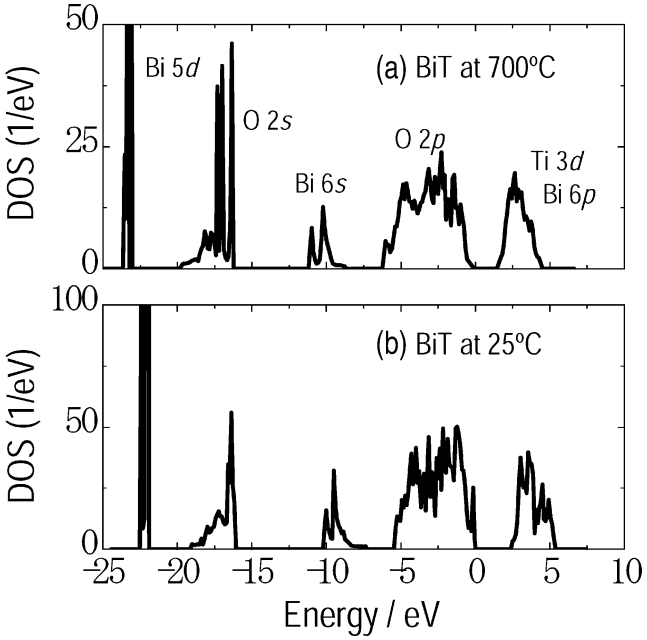

Fig. 4 Electronic density of states (DOS) of (**a**) the paraelectric phase at 700 °C and (**b**) the ferroelectric phase at 25 °C

states form the conduction band. [33, 34] The Bi 6*p* states overlap with the Ti3*d* states in the conduction band. The width of the calculated valence band is approximately 5.5 eV at the ferroelectric phase, which is in good agreement with the experimental value determined by soft-X-ray emission spectroscopy [35].

Figure 5 indicates the partial DOS (ion decomposed and sphere projected DOS) of the constituent ions. Although the orbital hybridization between the Ti 3*d* and the O 2*p* is clearly seen in both the paraelectric and the ferroelectric states, the significant difference in the hybridization by the ferroelectric transition is not detected. The partial DOS (PDOS) analysis shows a marked change in the orbital interaction between Bi and O induced by the transition. The primary band of the Bi 6*s* appears at around −10 eV, while that of the Bi 6*p* lies in the conduction band. The PDOS of the O 2*p* is observed to some degree in the Bi 6*s* band due to the hybridization of the Bi 6*s*–O2 *p*. Furthermore, the PDOS of the O 2*p* is seen also in the Bi 6*p* band caused by the Bi 6*p*–O 2*p* bonding and anti-bonding interaction.

In the Bi_2O_2 layers, the Bi2 6*s* is strongly hybridized with the O2 2*p* in both the paraelectric and ferroelectric states, and a large PDOS of the O2 2*p* is seen at the same energy level in the Bi2 6*s* main band. The Bi1 6*s*–O 2*p* hybridization is also recognized in both states. These results indicates that the traditional model [16, 18, 19, 21, 22, 36] based on the stereoactive lone-pair 6*s* electrons of Bi^{3+} is not sufficient to explain the structural distortion in the ferroelectric state.

3.3 Influence of ferroelectric phase transition

To understand the distorted crystal structure observed in the ferroelectric phase, bond valence analysis [37, 38] has been adapted. The bond valence (s_{ij}) [37] of a cation is defined by

$$s_{ij} = \exp\left[(l_0 - l_{ij})/B\right], \tag{2}$$

where, l_0 is bond valence parameter, l_{ij} is the distance between the cation and the adjacent anions, and B is the characteristic parameter (0.037 nm). The l_0 and B are empirical parameters that can be refined via use of the Inorganic Crystal Structure Database (ICSD). The bond valence sum (V_i) is expressed by

$$V_i = \sum\nolimits_i s_{ij}, \tag{3}$$

and, is assumed to be the static charge in the crystal structure. The V_{Ti2} was 4.2 in the paraelectric state at 700 °C, and Ti2 is overbonded in the octahedra. This indicates that the Ti2–O bonds are too short and the $Ti2O_6$ octahedra are under compressive stress. The ferroelectric phase transition resulted in the V_{Ti2} of approximately 4.0. This value is in good agreement with the nominal charge of Ti^{4+}, and the compressive stress in the $Ti2O_6$ octahedra is released in the ferroelectric state. In contrast, the ferroelectric transition led to an increase in V_{Ti1} from 4.0 (700 °C) to 4.3 (25 °C). In the ferroelectric state, Ti1 does not satisfy the bonding requirement, and is overbonded with the adjacent oxide ions.

The ferroelectric phase transition was found to result in a marked change in V_{Bi1} and V_{Bi2}. In the paraelectric state, Bi1 and Bi2 are characterized by strong underbonding.

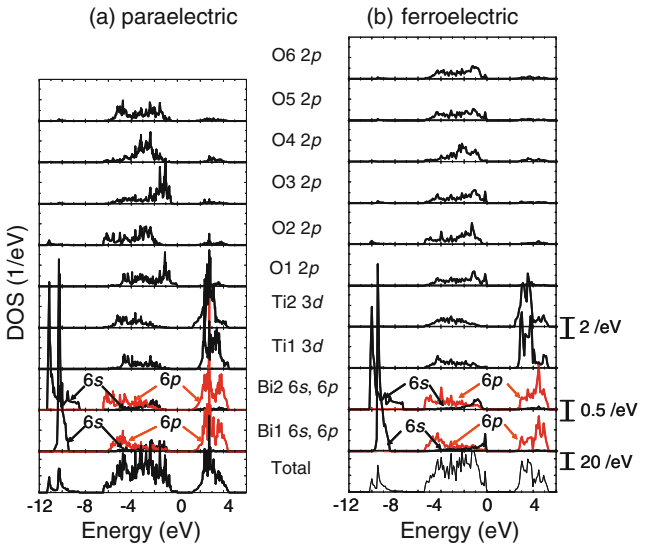

Fig. 5 Partial electronic density of states (PDOS) of (**a**) the paraelectric phase at 700 °C and (**b**) the ferroelectric phase at 25 °C

Especially, the underbonding of Bi1 is significant, and V_{Bi1} was 2.3 at 700 °C. This is much lower than the nominal charge of Bi^{3+}. This bond valence analysis exhibits that the chemical bonding of Bi1 with the adjacent oxide ions is not satisfied at the perovskite *A* site in the paraelectric state, and that Bi1 is eager to bond with oxide ions more tightly to satisfy its bonding requirement. The ferroelectric transition led to an increase in V_{Bi1} and V_{Bi2}. The values of V_{Bi1} and V_{Bi2} were 3.0 at 25 °C, which agrees well with the nominal charge of Bi^{3+}. While Bi1 cannot get a tight bonding with oxide ions in the paraelectric state due to the restricted movement only along the *c* axis in the *I*4/*mmm* structure, the descending symmetry due to the ferroelectric transition provides a three-dimensional degree of freedom for the displacements of Bi1 and Bi2 to fulfill their bonding requirement. The satisfactory bonding of Bi1 and Bi2 stabilizes the ferroelectric distortions in the crystal. It is strongly suggested that the loose bonding of Bi in the paraelectric state, especially the underbonded Bi1 with the neighboring oxide ions acts as the structural trigger for the ferroelectric transition in the BiT system. [20]

The selected bond lengths between Bi–O are listed in Table 1. In the paraelectric state, Bi is located at the high-symmetry 4*e* site. The ferroelectric transition led to several short bonds, and the satisfactory bonding of Bi1 is established. The shortest bond was seen between Bi1 and O3 ($l_{Bi1–O3}$) of 0.2284 nm along the *a* axis, which was 0.0458 nm (17%) smaller than that in the paraelectric state. The strong bonding of Bi1–O3 plays an essential role in the ferroelectric polarization as well as in the appropriate bond valence of the Bi1 at the *A* site. Shorter bonds were also found for $l_{Bi1–O3}$=0.2418 nm (12% shorter) along the *b* axis and $l_{Bi1–O1}$=0.2527 nm (17% shorter), which are responsible for the large TiO_6 octahedral rotation around the *a* axis, as clearly seen in Fig. 1(b).

Table 1 Selected bond lengths between Bi and O in the paraelectric (700 °C) and the ferroelectric states (25 °C).

	Ferroelectric state *T*=25 °C (nm)	Paraelectric state *T*=700 °C (nm)
Bi1–O1	0.2527 (7)	0.2976 (2)×4
Bi1–O1	0.2931 (7)	
Bi1–O1	0.2967 (7)	
Bi1–O1	0.3318 (7)	
Bi1–O3	0.2284 (6)	0.2742 (2)×4
Bi1–O3	0.2418 (6)	
Bi1–O3	0.3098 (7)	
Bi1–O3	0.3223 (7)	
Bi1–O5	0.2404 (6)	0.2530 (2)×4
Bi1–O5	0.2492 (7)	
Bi1–O6	0.2321 (7)	
Bi1–O6	0.3156 (7)	
Bi2–O2	0.2209 (5)	0.2324 (1)×4
Bi2–O2	0.2269 (5)	
Bi2–O2	0.2284 (5)	
Bi2–O2	0.2436 (6)	
Bi2–O4	0.2556 (5)	0.2889 (2)×4
Bi2–O4	0.2614 (5)	
Bi2–O4	0.3199 (6)	
Bi2–O4	0.3245 (6)	

It is interesting to note that a marked change in bond length was observed also for Bi2–O. The smallest two bonds were observed in $l_{Bi1–O4}$=0.2556 nm (12% shorter) along the *b* axis and $l_{Bi1–O4}$=0.2614 nm (10% shorter) along the *a* axis. These bond lengths are relatively longer compared with the shortest two $l_{Bi1–O3}$. Although the Bi2–O4 bonding contributes to the satisfactory bonding of Bi2 and to the stabilization of the alternative stacking of the Bi_2O_2 layers and the perovskite layers, these bonds are considered to play a minor role in the ferroelectricity in the BiT system.

We have calculated the electric charge within the sphere centered at the nuclei of all atoms, where the sphere radii, 0.1635 nm for Bi, 0.1323 nm for Ti, and 0.082 nm for O, are chosen to be the Wigner–Seitz radius. The electric charge of Bi 6*s* shows almost the same value (1.56 for Bi1 6*s* and 1.53 for Bi2 6*s*) for both ferroelectric and paraelectric phases. The change in electric charge of Bi2 6*p* (0.83) by the ferroelectric phase transition is not also observed. A significant change in electric charge is seen for Bi1 6*p*. The electric charge of Bi1 6*p* is 0.79 for the ferroelectric state, which is 0.12 larger than that for the paraelectric state (0.67). In a pure ionic model, Bi 6*p* states are present only in the conduction band, and PDOS of Bi 6*p* in valence band is zero. If the Bi 6*p* orbital is hybridized with O 2*p* orbital, PDOS of Bi 6*p* appears in the valence band as a result of bonding states of the orbital mixing. The much larger electric charge of Bi1 6*p* in the ferroelectric state clearly shows that the ferroelectric distortion is stabilized by the hybridization between Bi1 6*p*–O 2*p* stabilizes.

The ferroelectric phase transition leads to an increase in PDOS of the 2*p* state of O1 and O3. In the paraelectric state, the valence band maximum mainly consists of the O1 2*p* states, and the O3 2*p* states lie below the E_F. In contrast, the 2*p* states of O1, O3, and O5 that constitute the shorter bonds with Bi1 form the valence band maximum. Especially, the change in PDOS of O3 2*p* is significant in the vicinity of the E_F, which is consistent with the shortest bond length of Bi1–O3 in the ferroelectric state. These electronic and structural analyses demonstrate that the hybridization of the Bi1 6*s*–O3 2*p* acts as a trigger of the ferroelectric transition. This hybridization results in a satisfactory bonding of Bi1 at the *A* site, and then the ferroelectric distortion is stabilized in the perovskite layers.

4 Conclusions

The crystal structures of BiT in ferroelectric and paraelectric states have been investigated by the Rietveld analysis of neutron powder diffraction data, and the electronic band structure calculations have been performed to investigate the origin of ferroelectricity in BiT. The off-center Ti displacements in TiO_6 octahedra play a minor role in spontaneous polarization, while the entire shift of the TiO_6 octahedra with respect to the Bi ions results in a large spontaneous polarization along the *a* axis. The analysis of partial density of states and the electric charge within the sphere centered at the nuclei indicate that the ferroelectric transition leads to a strong hybridization between the Bi1 6*p* and the adjacent O 2*p* states. These structural and electronic band-structure analyses strongly indicate that the hybridization of the Bi 6*p*–O 2*p* in the perovskite layers is the trigger of ferroelectric transition in BiT, and that this hybridization is responsible for stabilizing the ferroelectric distortion in the perovskite layers.

References

1. S.Y. Wu, W.J. Takei, M.H. Francombe, Ferroelectrics **10**, 209 (1976)
2. Bengt Aurivillius, ARKIV FUER KEMI **1**, 499 (1949)
3. E.C. Subbarao, Phys. Rev. **122**, 804 (1961)
4. S.E. Cummins, L.E. Cross, J. Appl. Phys. **39**, 2268 (1968)
5. H. Irie, M. Miyayama, T. Kudo, J. Appl. Phys. **90**, 4089 (2001)
6. P.C. Joshi, A. Mansingh, M.N. Kamalasanan, S. Chandra, Appl. Phys. Lett. **59**, 2389 (1991)
7. W. Jo, G.C. Yi, T.W. Noh, D.K. Ko, Y.S. Cho, S.I. Kwun, Appl. Phys. Lett. **61**, 1516 (1992)
8. A.D. Rae, J.G. Thompson, R.L. Withers, A.C. Willis, Acta Crystallogr. B **46**, 474 (1990)
9. J.F. Dorrian, R.E. Newnham, M.I. Kay, D.K. Smith, Ferroelectrics **3**, 17 (1971)
10. T. Takenaka, K. Sakata, Ferroelectrics **38**, 769 (1981)
11. B.H. Park, B.S. Kang, S.D. Bu, T.W. Noh, J. Lee, W. Jo, Nature **401**, 682 (1999)
12. T. Kojima, T. Sakai, T. Watanabe, H. Funakubo, K. Saito, M. Osada, Appl. Phys. Lett. **80**, 2746 (2002)
13. H. Uchida, H. Yoshikawa, I. Okada, H. Matsuda, T. Iijima, T. Watanabe, T. Kojima, H. Funakubo, Appl. Phys. Lett. **81**, 2229 (2002)
14. H. Matsuda, S. Ito, T. Iijima, Appl. Phys. Lett. **83**, 5023 (2003)
15. M. Soga, Y. Noguchi, M. Miyayama, H. Okino, T. Yamamoto, Appl. Phys. Lett. **84**, 100 (2004)
16. R.E. Newnham, R.W. Wolfe, J.F. Dorrian, Mater. Res. Bull. **6**, 1029 (1971)
17. R.L. Withers, J.G. Thompson, A.D. Rae, J. Solid State Chem. **94**, 404 (1991)
18. B. Frit, J.P. Mercurio, J. Alloys Compd. **188**, 27 (1992)
19. L. Nistor, G. Vantendeloo, S. Amelinckx, Phase Transit. **59**, 135 (1996)
20. C.H. Hervoches, P. Lightfoot, Chem. Mater. **11**, 3359 (1999)
21. Y. Shimakawa, Y. Kubo, Y. Tauchi, H. Asano, T. Kamiyama, F. Izumi, Z. Hiroi, Appl. Phys. Lett. **79**, 2791 (2001)
22. Q.D. Zhou, B.J. Kennedy, C.J. Howard, Chem. Mater. **15**, 5025 (2003)
23. Y. Noguchi, I. Miwa, Y. Goshima, M. Miyayama, Jpn. J. Appl. Phys. **39**, L1259 (2000)
24. Y. Noguchi, M. Miyayama, Appl. Phys. Lett. **78**, 1903 (2001)
25. T. Kamiyama, K. Oikawa, F. Izumi, M. Kosaka, H. Onodera, Y. Yamaguchi, M. Kasaya, K. Kojima, Physica, B **241**, 376 (1997)
26. T. Ohta, F. Izumi, K. Oikawa, T. Kamiyama, Physica, B **234**, 1093 (1997)
27. J.P. Perdew, K. Burke, M. Ernzerhof, Phys. Rev. Lett. **77**, 3865 (1996)
28. J.P. Perdew, K. Burke, Y. Wang, Phys. Rev. B **54**, 16533 (1996)
29. P.E. Bloechl, Phys. Rev. B **50**, 17953 (1994)
30. G. Kresse, D. Joubert, Phys. Rev. B **59**, 1758 (1999)
31. G. Kresse, J. Furthmuller, Phys. Rev. B **54**, 11169–11186 (1996)
32. W. Zhong, R.D. Kingsmith, D. Vanderbilt, Phys. Rev. Lett. **72**, 3618 (1994)
33. T. Higuchi, M. Tanaka, K. Kudoh, T. Takeuchi, Y. Harada, S. Shin, T. Tsukamoto, Jpn. J. Appl. Phys. **40**, 5803 (2001)
34. T. Higuchi, K. Kudoh, T. Takeuchi, Y. Masuda, Y. Harada, S. Shin, T. Tsukamoto, Jpn. J. Appl. Phys. **41**, 7195 (2002)
35. T. Higuchi, Y. Moriuchi, Y. Noguchi, M. Miyayama, S. Shin, T. Tsukamoto, Japanese Journal of Applied Physics Part 1-Regular Papers Short Notes & Review Papers **42**, 6226 (2003)
36. J.G. Thompson, A.D. Rae, R.L. Withers, D.C. Craig, Acta Crystallogr., B Struct. Sci. **47**, 174 (1991)
37. I.D. Brown, D. Altermatt, Acta Crystallogr., B Struct. Sci. **41**, 244 (1985)
38. M. Okeeffe, Struct. Bond. **71**, 161 (1989)